Substrate-Induced Variations of Molecular Packing, Dynamics, and Intermolecular Electronic Couplings in Pentacene Monolayers on the Amorphous Silica Dielectric

Lucas Viani,[†,⊥] Chad Risko,[†,*] Michael F. Toney,[‡] Dag W. Breiby,[§] and Jean-Luc Brédas[†,∥,*]

[†]School of Chemistry and Biochemistry and Center for Organic Photonics and Electronics, Georgia Institute of Technology, Atlanta, Georgia 30332-0400, United States, [‡]Stanford Synchrotron Radiation Lightsource, SLAC National Accelerator Laboratory, Menlo Park, California 94025, United States, and [§]Department of Physics, Norwegian University of Science and Technology, Høgskoleringen 5, 7491 Trondheim, Norway. [⊥]Present address: Dipartimento di Chimica e Chimica Industriale, Università di Pisa, Via Risorgimento 35, 56126 Pisa, Italy. [∥]Also affiliated with Department of Chemistry, King Abdulaziz University, Jeddah 21589, Saudi Arabia.

ABSTRACT Charge-carrier transport in thin-film organic field-effect transistors takes place within the first (few) molecular layer(s) of the active organic material in contact with the gate dielectric. Here, we use atomistic molecular dynamics simulations to evaluate how interactions with bare amorphous silica surfaces that vary in terms of surface potential influence the molecular packing and dynamics of a monolayer pentacene film. The results indicate that the long axis of the pentacene molecules has a non-negligible tilt angle away from the surface normal. Grazing-incidence X-ray diffraction patterns for these models are calculated, and we discuss notable differences in the shapes of the Bragg rods as a function of the molecular packing, also in relation to previously published experimental reports. Intermolecular electronic couplings (transfer integrals) evaluated for the monolayers show marked differences compared to bulk crystal calculations, a result that points to the importance of fully considering the molecular packing environment in charge-carrier mobility models for organic electronic materials.

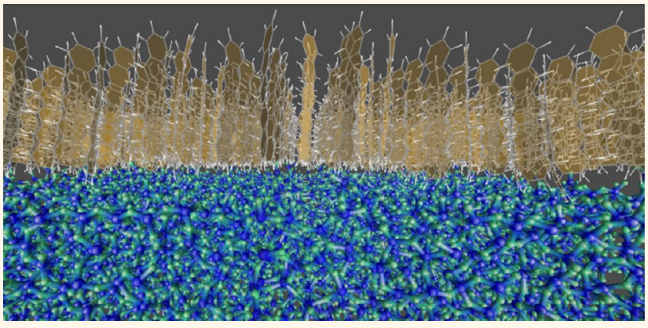

KEYWORDS: organic–inorganic interface · charge-carrier transport · X-ray scattering simulations

The device-level characteristics of thin-film electronic and optoelectronic devices where the active layers are composed of π-conjugated organic molecules and polymers—including organic field-effect transistors (OFETs), light-emitting diodes (OLEDs), and photovoltaics (OPVs)—are often dictated by the many buried materials interfaces within the device architecture. The manner with which molecules arrange themselves at these interfaces impacts the intrinsic geometric and electronic properties of individual molecules as well as the strength of intermolecular electronic communication among neighboring molecules and any adjacent substrate. Such considerations, therefore, must be taken into account during the molecular design process should one want to truly control final materials-scale properties through synthetic chemistry.

Focusing here on OFETs, detailed molecular and nanoscale information pertaining to the interface between the active layer and the dielectric (whether the dielectric is an inorganic- or organic-based material) is vital to the realization of thin-film devices with enhanced operating efficiencies; it allows, for instance, the development of materials and device architectures to maximize charge-carrier injection, transport, and collection.[1,2] In particular, since charge-carrier

* Address correspondence to chad.risko@chemistry.gatech.edu; jean-luc.bredas@chemistry.gatech.edu.

Received for review October 13, 2013 and accepted December 26, 2013.

Published online December 26, 2013
10.1021/nn405399n

transport takes place within the first few molecular layers nearest the dielectric[3−5] and as this process is heavily dependent on the degree of the intermolecular electronic couplings (transfer integrals),[2] an *a priori* understanding of how the molecules pack at the interface is indispensable.

While there are now hundreds of materials designed for either p-channel (where the charge carrier is a hole) or n-channel (where the charge carrier is an electron) transport,[6−12] pentacene continues to serve as a benchmark system due to good thin-film p-channel transport on a number of dielectrics,[13−16] including amorphous silica (αSiO_2).[17,18] In addition, there has been considerable experimental and theoretical work to characterize the structural properties of pentacene thin films as a function of these dielectric interfaces,[16,17,19−23] for both mono- and multilayer films. The nature of the surface on which pentacene is deposited has an influence on the molecular packing, either favoring a flat/parallel (on, for example, graphene, Cu, and Au)[24−26] or upright/perpendicular arrangement (on polymethylmethacrylate [PMMA], Si, and αSiO_2)[15,17,27] with respect to the substrate.

A variety of X-ray diffraction and atomic force microscopy experiments have established that the (long axis) height of an upright pentacene molecule on αSiO_2 ranges from 14.0 to 16.0 Å,[27−33] suggesting that the long axis of the pentacene molecules orient (nearly) perpendicular to the αSiO_2 surface. Grazing-incidence X-ray diffraction (GIXD)[17,27] experiments reveal further information concerning the relative pentacene orientations within the herringbone packing configurations by allowing for the decomposition of the total tilt angle along the *a* and *b* crystallographic axes (these axes are parallel with respect to the αSiO_2−pentacene interface); the decomposition is denoted here as [ψ_a, ψ_b], where the total tilt ψ_{tot} is defined by $\cos(\psi_{tot}) = \cos(\psi_a)\cdot\cos(\psi_b)$; see Figure 1b. Differences in terms of the respective long-axis tilt angles and decomposition have been ascertained and are proposed to be a function of the thickness of the pentacene films formed: for instance, the total long-axis pentacene tilt angle for a 48 nm (fiber-structured) thin film is 8.2° with a decomposition of [5.6°, 6.0°] and layer height of 15.4 Å;[27] on the other hand, pentacene molecules at submonolayer coverage stand perfectly upright (0° tilt and a decomposition of [0°, 0°]) with a layer height of 16.0 Å.[17] These differences in tilt angle and layer height, while modest, have been suggested to arise from shorter *a* axis length; for submonolayer coverage, it is on the order of 5.90−5.92 Å compared to 5.96 Å in the thin-film phase. Notably, both of these *a* axes are much shorter than the bulk *a* axis (6.27 Å).[17]

Here, our aim is to employ atomistic molecular dynamics (MD) simulations to investigate the molecular packing and dynamics of pentacene monolayers on

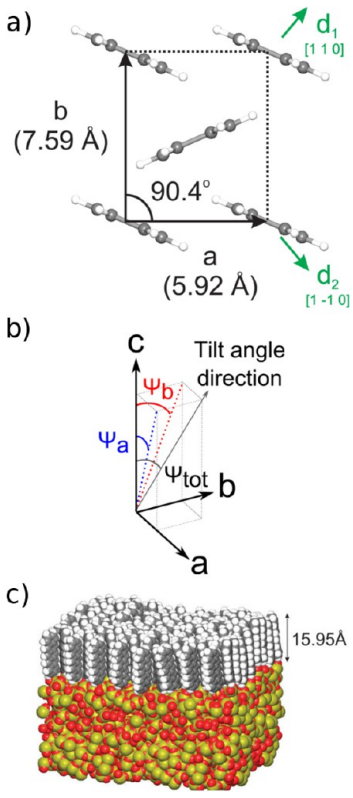

Figure 1. (a) Dimensions of the monolayer pentacene unit cell[17] used in this work and (b) a pictorial representation of the tilt angle decomposition. (c) Representative snapshot of the αSiO_2−pentacene interface (substrate 3, see below) after a 2.5 ns MD simulation.

αSiO_2. As a first step, we consider the bare αSiO_2 interface, which has implications concerning the nature of the available packing configurations. Calculated grazing-incidence X-ray diffraction patterns based on the atomistic models reveal notable differences in the shapes of the Bragg rods as a function of the molecular packing. We then examine how differences in the monolayer morphologies affect the intermolecular electronic couplings (transfer integrals), which show marked differences compared to bulk crystal calculations. These results point to the importance of fully considering the molecular packing environment in charge-carrier mobility models for organic electronic materials. A major result of our study is that surface inhomogeneity at the nanometer scale, the scale over which the simulations were performed, can have considerable impact on monolayer packing and thus on charge-carrier transport in thin-film organic electronic materials.

RESULTS AND DISCUSSION

αSiO_2 Slab Morphologies. Through the simulation procedure described in detail in the Computational Methodology section, we prepared four bulk αSiO_2 samples that were then cut to produce the αSiO_2 slabs. The four bulk αSiO_2 samples feature very similar average values with respect to the Si−O bonds (1.64 Å) and O−Si−O angles (109.0°), which are in good agreement with

experiment (1.62 Å and 109.3°, respectively).[61] We do note a small deviation of the Si−O−Si angles with respect to experiment; experimentally the Si−O−Si angle distribution is 120.0−180.0° with a median of 144.0°,[61] while the COMB-simulated morphologies provide Si−O−Si angles that span 110.0−160.0° with a median of 135.6°.

The surface roughness for the slabs cut from the bulk samples was estimated using the rolling sphere technique[62] with a probe radius of 1.7 Å. The surface roughness was found to range from 2.0 to 2.5 Å. In prior studies on the influence of dielectric roughness on the performance of pentacene thin-film transistors (TFTs), such degrees of surface roughness have been considered "smooth" with respect to experimental measurements.[19] The charge distributions of the O and Si atoms are described by narrow Gaussian distributions centered at −1.47 |e| and +2.88 |e|, respectively. As we discuss below, the charge distribution at the slab surface plays a substantial role in the morphology of the pentacene monolayers; we note that in these SiO_2 realizations there is a stochastic overrepresentation of oxygen atoms at the surface.

αSiO$_2$−Pentacene Monolayer Interface. The results of the αSiO$_2$−pentacene-monolayer interface simulations (Figure 2) show good agreement with estimated experimental values for the pentacene layer height (14.5−16.0 Å), with mean layer heights of 15.75 ± 0.61 Å (**1**), 15.70 ± 0.59 Å (**2**), 15.95 ± 0.84 Å (**3**), and 15.72 ± 0.28 Å (**4**), where the numbers (**1**−**4**) refer to the different αSiO$_2$ slabs (see Section 2.1). It is clear by visual inspection that the pentacene molecules are arranged in a mostly upright orientation with respect to the αSiO$_2$ surface (see Figure 1c). The mean total tilt angles on the four surfaces—15.3 ± 0.8° (**1**), 15.8 ± 0.9° (**2**), 11.7 ± 1.0° (**3**), and 15.7 ± 0.8° (**4**)—are clearly not zero, although the results are in accord with previous theoretical evaluations.[22,32] The (average) monolayer heights and molecular tilt angles (after equilibration) show little change with time (Figure 2).

At this stage, it is of interest to compare aspects of the simulations employed here with those of previous studies. Our simulations, as noted above, make use of intermolecular non-Coulomb terms that are validated against crystalline structures and intermolecular vibrations of pentacene polymorphs, while electrostatic interactions are carried out with 2D Ewald summations. Periodic boundary conditions are used to reduce boundary effects, and the pentacene molecules sare allowed full flexibility (*i.e.*, the pentacene molecules are not enforced to be rigid). Finally, the αSiO$_2$ slabs are atomistic models with equilibrated charges (from bulk simulations that reproduce well the properties of bulk αSiO$_2$),[55−57] which allow us to take into account differences in surface roughness and electrostatic potentials (see below). The use of a fully atomistic study is aligned with the earlier work of Della Valle and co-workers,[22] who adopted models that employ

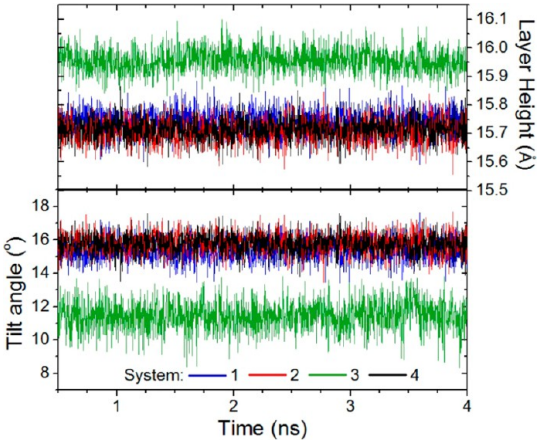

Figure 2. Layer height (top) and the total tilt angle (bottom) fluctuations with time during the MD simulations. The colors refer to the silica slabs as indicated.

clusters of rigid pentacene molecules in either bulk-like or thin-film-like configurations on atomistic αSiO$_2$ slabs. The bulk-like configuration was shown to be stable throughout the simulations, while the tilt angle distributions for the thin-film configuration broadened with time. Simulations by Yoneya and co-workers,[23] importantly, resulted in nontilted (perpendicular) pentacene orientations for periodic monolayers, which then showed increased tilt with increased number of pentacene layers. However, these authors considered the αSiO$_2$ surface *via* a nonatomistic representation (*i.e.*, through a Lennard-Jones (9−3) potential), and both the noncovalent and electrostatic interactions among the pentacene molecules were given different forms from those used here. A feature of our work is that the simulations are fully atomistic with the aim to simulate monolayers with as few constraints as possible. This is of importance, as differences in the surface (and/or surface termination) can lead to significant changes in film orientation (see below).

Although the total tilt angles indicate a mostly upright pentacene orientation in the monolayer, these values are larger than those derived from the (submonolayer coverage) GIXD experiments. The total tilt angle is a property that describes the overall molecular orientation and provides no insight concerning either the direction of the molecular tilt or the molecular dynamics. In order to better compare the calculated and experimental values, we analyzed the tilt angle components and their fluctuations in time. We observe a mean decomposition across all pentacene molecules in the simulated monolayers ($[\psi_a, \psi_b]$ along the *a* and *b* axes, respectively) of [15.0°, 0.5°] (**1**), [2.0°, 15.2°] (**2**), [11.3°, 0.9°] (**3**), and [0.0°, 14.9°] (**4**), where **1** and **3** are in agreement with previous theoretical estimates of [11.0°, 0.0°].[32] Interestingly, the tilt-angle decomposition indicates that the molecules tilt preferentially along the *a* axis on surfaces **1** and **3** and along the *b* axis on surfaces **2** and

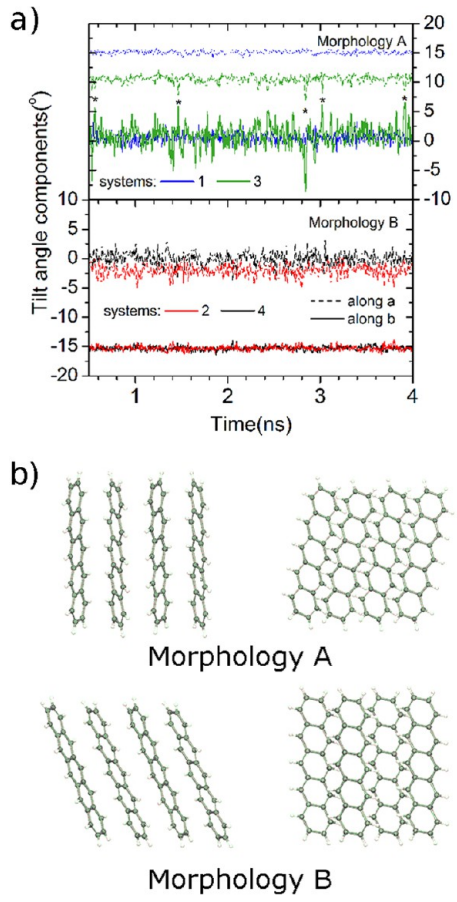

Figure 3. (a) Fluctuation in time of the average total tilt angle and its components along *a* and *b* for samples 1 and 3 (top) and 2 and 4 (bottom). (b) Illustration of the A (substrates 1 and 3) and B molecular packing configurations (substrates 2 and 4). The peaks indicated by stars characterize group motions induced by intermolecular interactions.

4 (see Figure 3b). Although tests with larger systems show similar results, we emphasize that the homogeneity of the tilt angle values may be reinforced by the periodic boundary conditions. For the remainder of this work we will refer to these two types of morphologies as **A** and **B**, respectively. Analysis of the tilt-angle component evolution with time (see Figure 3a) shows that the molecular tilt is nearly constant throughout the 4 ns simulations, although dynamical deviations of up to ~5° are observed for the larger tilt-angle component compared to ~2° for the smaller angle with standard deviations (σ) ranging from 1° to 3°. Notably, these tilts differ quite substantially from the experimental estimates of [5.6°, 6.0°][27] and [0°, 0°],[17] even though the experimentally estimated monolayer heights (15.4 and 16.0 Å, respectively) are comparable to the heights determined here. We recall that the pentacene molecules in our simulations were allowed full flexibility and not kept rigid as in refs 17 and 22, thus allowing full accommodation of the pentacene molecules within the layer.

It is therefore of interest to investigate further the nature of these differences with previous results, especially as a function of the simulated αSiO_2 surfaces. In an attempt to verify the dependence of the molecular tilt on the nature of the different αSiO_2−pentacene monolayer interactions, the substrates that produced pentacene monolayers of type **A** were exchanged with those that gave type **B**; the switched systems were then equilibrated for 4 ns. Interestingly, changing the underlying substrate drove the orientation of the pentacene monolayer to the other configuration; that is, the monolayer with the **A**-type morphology was driven to the **B**-type morphology by the αSiO_2 surface that initially produced the **B** morphology, and *vice versa*.

The origin of the **A** and **B** morphologies results from a competition between the pentacene/pentacene and pentacene/αSiO_2 interactions. As a first gauge of possible differences among the slabs that could be driving these morphological changes, the electrostatic potential of the surface experienced by the pentacene molecules (at a distance 10 Å above the αSiO_2 slabs) was examined (Figure 4). Substantial differences among the simulated substrates were found, with slabs **1** and **3** having more negative character; although all four surfaces have large oxygen content at the interface, the oxygen atom densities in **1** and **3** are larger than in **2** and **4**. Importantly, the surfaces that lead to the **A** pentacene configuration display average electrostatic potentials (C_{pot}), based on the equilibrated COMB atomic charges at 10 Å from the surface, of −10.0 V (**1**) and −14.7 V (**3**), while the surfaces that lead to the **B** configuration display potentials of −1.5 V (**2**) and +3.9 V (**4**).

To gain more insight into these results, additional MD simulations were performed setting the charges of all Si and O to zero, thus mimicking a neutral (uncharged) surface. In this scenario, the molecules on all substrates pack in a fashion that is equivalent to the **A** morphology; we note that morphology **A** is ~1.0 meV/molecule (0.13 eV for 128 molecules) more energetically favorable than **B**. These results indicate that surfaces with high oxygen content (fully negative surface potential) and neutral surfaces induce packing configuration **A** and those either with fully positive surface potential due to large silicon content (**4**) or with mixed positive and negative areas (**2**) induce configuration **B**.

It is of interest to understand how differences among the empirical and theoretical tilt angles might manifest themselves in GIXD patterns, as this is a key experimental technique for the investigation of thin-film structures.[17,27,32,63] The intensity patterns were calculated using SimDiffraction,[64] assuming Cu Kα radiation (λ = 1.542 Å), an incidence angle of 0.2°, and a peak width of 0.015 $Å^{-1}$ accounting for both the intrinsic width and instrumental broadening. Lorentz and polarization corrections were included as described elsewhere. Notably, refraction effects were

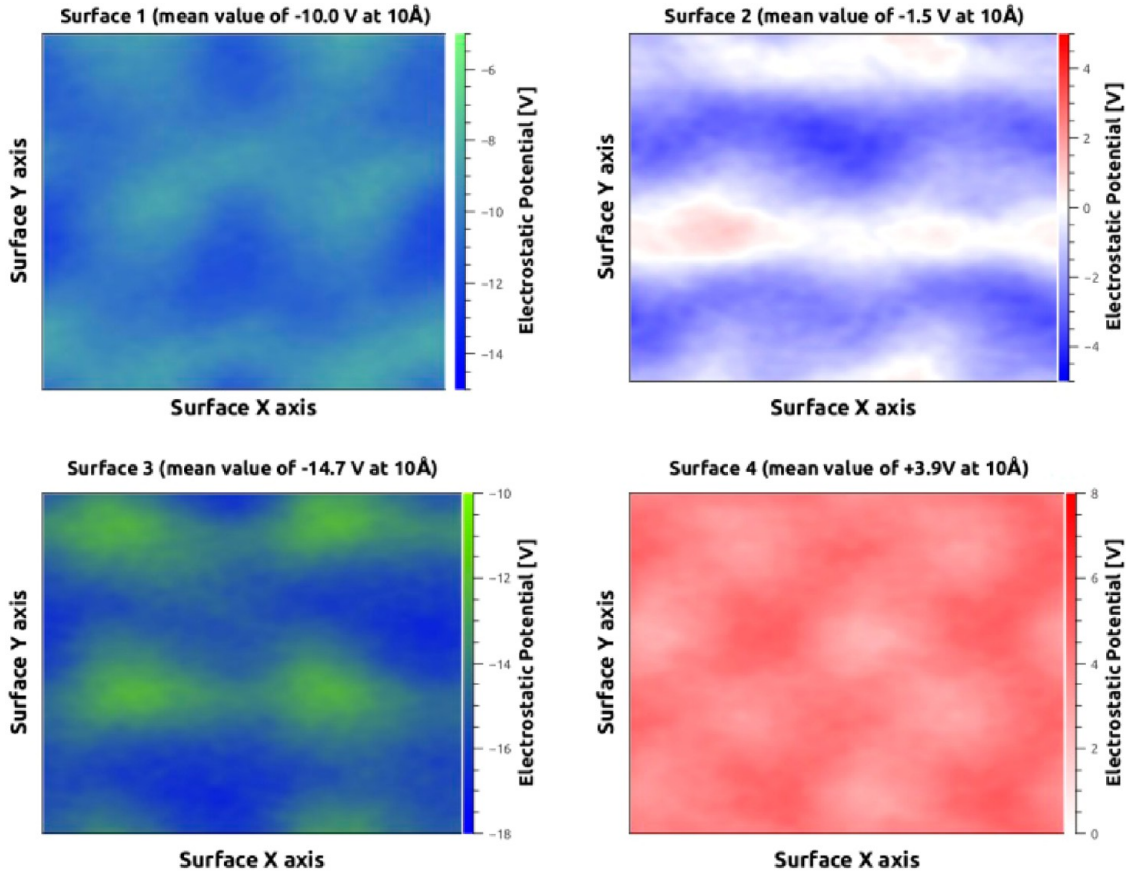

Figure 4. Electrostatic potential landscape of the four αSiO_2 surfaces determined at a distance 10 Å above the αSiO_2 slabs.

included, giving rise to the Vineyard[65] feature of increased intensity just above the sample horizon (*cf.* Figure 4 and Figure 5). For the MD structures, corresponding GIXD patterns were calculated assuming that the MD structures are representative for domains in the monolayer structure with random in-plane orientations, referred to as "2D powder". Following basic scattering theory, the Bragg peak positions from the 2D structure are defined by the unit-cell dimensions a, b, and γ. Because the previously published unit-cell dimensions for a pentacene monolayer[17] were used as a constraint in the MD simulations, the calculated Q_{xy} positions of the peaks thus necessarily match the experimental data. For a monolayer, there is no repetition in the out-of-plane direction, leading to so-called Bragg rods extending along Q_z in reciprocal space.[66] The intensity distributions along the Bragg rods depend on the molecular decoration of the unit cell. As anticipated from the considerable total tilt given by the MD results and the qualitative difference between the **A** and **B** structures, the calculated scattering patterns are qualitatively different. Figure 5 shows GIXD simulations for the **A** (substrate **3**) and **B** (substrate **4**) structures and also for a unit cell containing perfectly upright pentacene molecules. The simulated scattering pattern based on the perfectly upright structures shows good qualitative agreement with the experimental scattering pattern published by Mannsfeld and coworkers,[17] as expected. Likewise, for the (tilted) **A** and **B** structures, the simulated patterns differ significantly from the experimental pattern, with a more complex Q_z behavior of the Bragg rods.

The differences in the simulated GIXD patterns suggest that one should readily be able to discriminate these different structures with current experimental accuracy. However, it has proven challenging to distinguish the patterns of a perfectly perpendicular orientation from those with a total tilt angles ψ_{tot} varying by less than a few degrees (Figure 6). For $\psi_{tot} = 3°$, the variation between the intensity patterns obtained for different decompositions is rather small, appearing to be within the experimental uncertainty of published work,[17,27] and to experimentally distinguish between these and related monolayer models could thus be challenging. As expected, for a larger total tilt of $\psi_{tot} = 5°$, the differences between the scattering patterns become more significant, and the intensity variations as a function of decomposition both within specific Bragg rods and between the rods facilitate discriminating between different models. These considerations emphasize the need to report uncertainty when describing detailed molecular models based on GIXD. Statements like "the molecules are oriented edge-on" should hence be regarded as approximate.

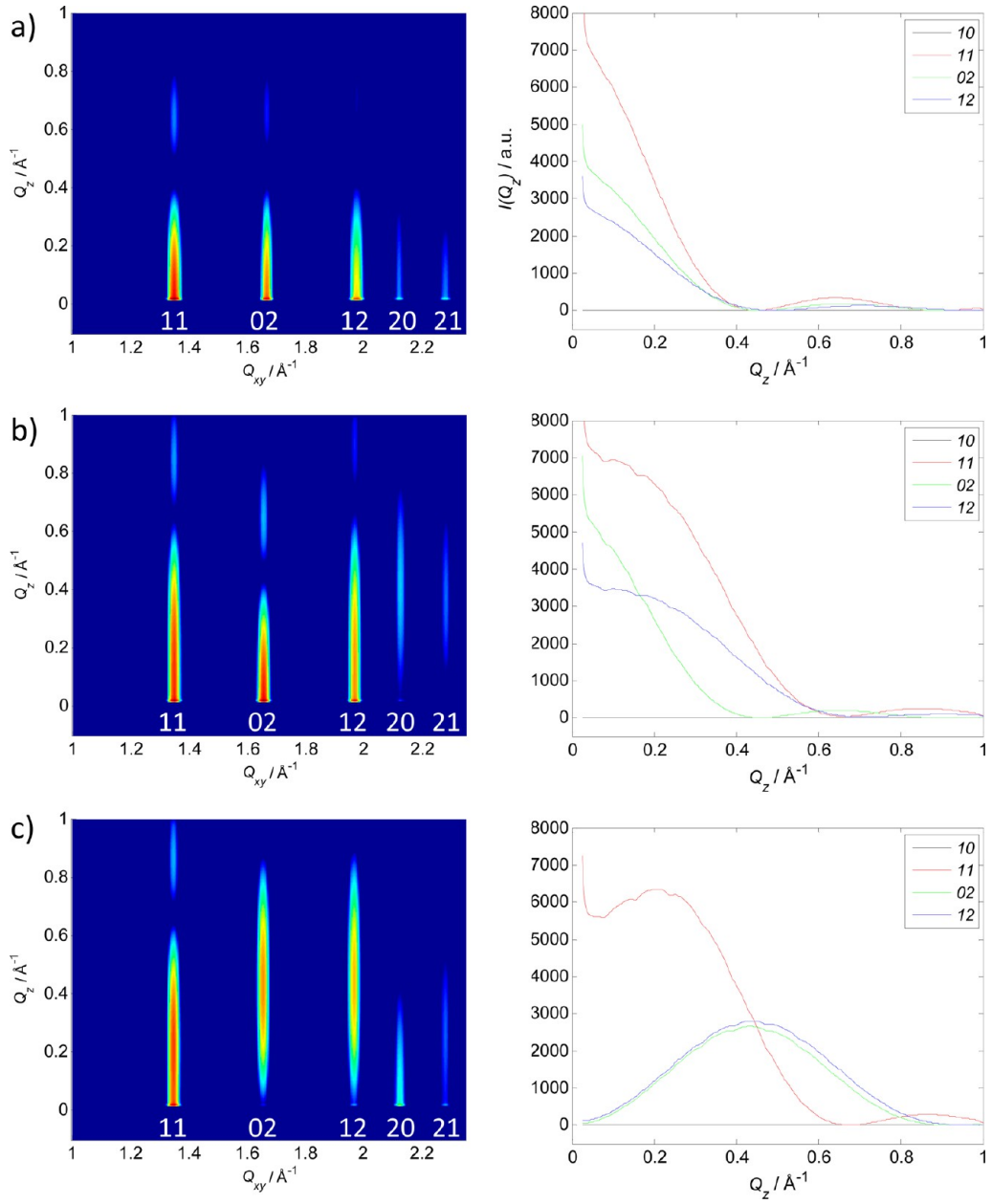

Figure 5. [Left] Calculated GIXD patterns based on the atomic coordinates of the simulated monolayer systems and [right] plot of the intensity along the Bragg rods in the simulated GIXD patterns to the left for (a) the upright morphology corresponding to a unit cell with two pentacene molecules oriented perpendicular to the surface and (b, c) systems 3 and 4, respectively.

These results, in total, suggest that seemingly minor (experimental and theoretical) nonuniformities in the surface structure—and in particular as shown here the electrostatic interactions at the bare αSiO_2 interface—can lead to substantial morphological changes of a molecular monolayer at the nanometer length scale. From the perspective of molecular dynamics simulations, great care should be taken in the preparation and reporting of simulated surfaces, as seemingly modest differences can lead to strikingly different interpretations of the nature of such interfaces.

An important aspect as well will be to examine how different surface treatments, *e.g.*, through hydrogen atom termination or the presence of water molecules on the surface, can contribute to resolving the discrepancy between the larger theoretically determined tilt angles (both here and in refs 22 and 32) compared to those reported by GIXD experiments,[17,27] and more generally how to tune molecular structures on surfaces. For example, priming the substrate with a monolayer of octadecyltrichlorosilane is a frequently used method to increase the performance of organic field-effect transistors,[67] which we anticipate will be better understood in the future using the methods described here.

Intermolecular Electronic Coupling as a Function of Molecular Packing in the Monolayer. It is of interest to consider how

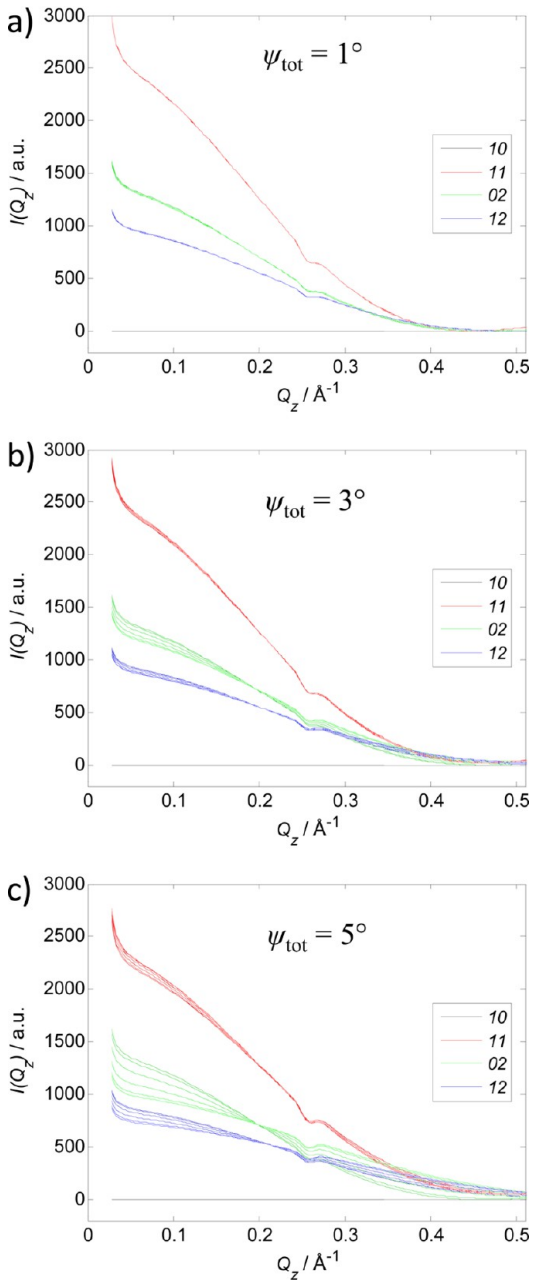

Figure 6. Simulated GIXD, using an "idealized" unit cell of fully upright standing molecules as a starting point, to investigate the sensitivity of the scattering patterns to changes in molecular tilt. The two molecules decorating the (fixed size) unit cell were both tilted by the same angle ψ_{tot}, about an in-plane axis oriented at φ_{ip} with respect to the unit-cell *a* axis. The angle φ_{ip} is thus directly related to the decomposition and was varied in steps of 18°.

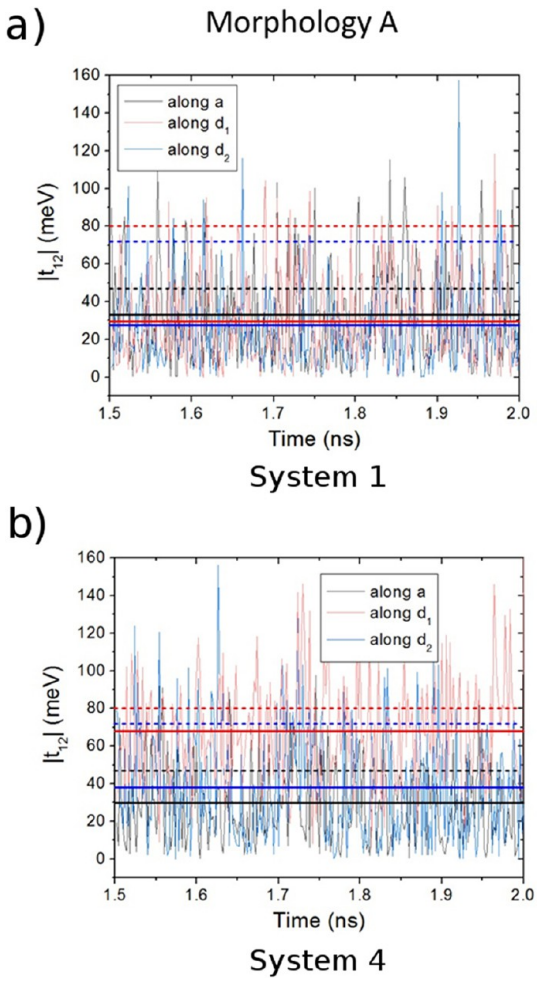

Figure 7. Fluctuations of the electronic couplings for holes computed for a randomly chosen pair of pentacene molecules in systems 1 (morphology A) and 4 (morphology B) along the *a* axis and *d1* and *d2* directions (Figure 1a for definitions). The mean value along each direction is indicated by the horizontal solid lines. The horizontal dashed lines indicate the transfer integral values calculated for a perfect molecular crystal.[70]

the structural differences between the monolayer and the bulk influence charge-carrier transport; this can be accomplished by evaluating the amplitudes of the intermolecular electronic couplings (transfer integrals) *t*.[68] Since the electronic couplings are highly sensitive to both the relative spacings and spatial orientations of neighboring molecules,[1,69] we expect different electronic couplings arising from the **A** and **B** monolayer morphologies.[21] Furthermore, the dynamic variations (on the order of 5°) in the molecular tilt angle ψ_{tot} will have considerable impact. Intermolecular electronic couplings were calculated using the same approach as described in ref 70, where the semiempirical Hartree–Fock INDO method (as developed by Zerner and coworkers[71,72]) was used to describe intermolecular electronic interactions.

Figure 7 shows the fluctuation of the absolute value of *t* for hole (p-channel) transport during a 500 ps window of the MD simulation for a randomly chosen pair of pentacene molecules along the axis *a* (t_a) and the dominant *d1* (t_{d1}) and *d2* (t_{d2}) transport directions (see Figure 1a for definitions). In all systems, a large and fast oscillation of the absolute value of the electronic coupling is observed that ranges from 0 to 160 meV, a result that reflects the changes in the dimer conformation due to the molecular motions. The mean values of t_a, t_{d1}, and t_{d2} are indicated by the horizontal solid lines

in Figure 7. The average electronic couplings along the *a* axis (32 meV) and *d2* direction (33 meV) are similar in the four monolayer structures studied here. These electronic couplings are about 15 and 39 meV smaller, respectively, than those determined at the same level of theory for the perfect (bulk) molecular crystal.[70] The electronic couplings along *d1* experience a much stronger impact due to the changes in packing induced by the different αSiO_2 surfaces: *t* is two times larger for morphology **B** (62 meV) *versus* **A** (31 meV). These results, as one might expect, reveal how changes to the molecular packing—driven mainly by the surface/monolayer interactions—can have a substantial impact on the charge-carrier properties of the organic semiconductor. The t_a, t_{d1}, and t_{d2} values for the perfectly upright geometry are 64, 31, and 56 meV, respectively, falling within the range derived for the bulk and tilted monolayer morphologies. These findings suggest that higher mobilities may be achieved by manipulating the αSiO_2−pentacene interface interactions through variations in processing to induce different molecular packings, as was realized experimentally by Bao and co-workers.[73]

CONCLUSIONS

We have explored how variations in the electrostatics of αSiO_2 surfaces influence the molecular packing and dynamics of pentacene monolayers. We obtain mean monolayer heights on the simulated αSiO_2 surfaces in the range 15.70−15.95 Å, which are in good agreement with the available experimental estimates. Mean tilt angles in the range 11.0−15.8° were calculated as a function of the chemical and electrostatic variations in the αSiO_2 surfaces. These values are larger than the experimental results derived from GIXD experiments,[17,27] yet agree with previous theoretical assessments.[22,32] Two predominant morphologies were obtained for the monolayer, which we find are related to the surface electrostatics. The energetically favored structure is found to feature the smallest intermolecular electronic couplings. These findings suggest that higher mobilities may be achieved by manipulating the αSiO_2−pentacene interactions.

Importantly, we directly compared our results with experimental GIXD patterns by using the atomistic models as input for GIXD calculations and explored how modest changes to the tilt angles result in variations in the GIXD pattern. From a molecular dynamics simulations standpoint, we note that there is a need to continue to strive for direct validation by comparison with experiment. For example, one often finds the terms "thin-film" and "bulk" phase used in the literature to describe the structure of pentacene. This terminology, however, is rather broad and imprecise, as can be seen here through the wide variation in the tilt angle components. Moreover, the variation in the pentacene monolayer structure and computed intermolecular electronic couplings as a function of seemingly modest changes in the properties of the bare αSiO_2 surfaces reveal the importance of accurately taking into account the environmental effects.

To conclude, we have obtained qualitative agreement with available experimental data concerning the morphology of the αSiO_2−pentacene interface. A key finding is that the details of the αSiO_2 surface, such as the roughness[74,75] and the surface potential, can have tremendous impact on the molecular packing, which in turn can greatly affect the charge-carrier transport properties at the organic−dielectric interface. Various types and degrees of surface termination—either by hydrogen atoms or adsorption of water molecules—available if the αSiO_2 surface is exposed to air were not considered here, yet could play a significant role in the resultant film morphology.

COMPUTATIONAL METHODOLOGY

A series of αSiO_2−pentacene interfaces were prepared through a multistep molecular-dynamics procedure. First, a bulk amorphous silica sample was prepared using the cristobalite polymorph. This bulk sample was then cleaved and relaxed to form a series of four bare αSiO_2 slabs. Pentacene monolayers were then placed on these slabs, their atomic positions were allowed to equilibrate, and the dynamics were evaluated. We describe the procedure in more detail in the following sections.

Simulation of the Silica Glass Surface. The simulations of αSiO_2 were performed using the charge-optimized many-body (COMB)[34,35] potential as implemented in the LAMMPS software suite.[36] This potential has demonstrated reliability for the description of many properties, including the local order of the condensed phase of silicon and silica polymorphs.[35] In the particular case of quartz silica, the COMB potential provides morphologies that well reproduce the main structural properties of amorphous SiO_2.[37,38] The use of charge-equilibrated potentials is key in the simulation of electrostatic interactions at interfaces, since different regions on the surface will feature slightly different charges, thus directly affecting the local electrostatic interactions with the monolayer molecules.[34,35] These differences are further amplified in the case of amorphous compounds.[37,38]

Periodic slabs of amorphous silica have been derived through a variety of procedures.[22,39−43] In this work, we started with a 4 × 4 × 4 supercell of the crystalline cristobalite polymorph,[44] corresponding to a cubic box 28.55 Å long, that contains 1536 atoms and has a density of 2.18 g/cm^3 (similar to that for amorphous silica, 2.20 g/cm^3).[39,40] Using a canonical NVT ensemble (constant number of atoms *N*, volume *V*, and temperature *T*), the crystalline silica was heated from 300 to 4000 K in 80 ps with time steps of 1 fs. The temperature was kept constant at 4000 K for 70 ps in order to allow all the atoms to diffuse and lose memory of their original positions. A new unit cell, preserving the density of amorphous SiO_2 and constrained to the experimentally determined pentacene monolayer unit-cell dimensions on αSiO_2 (a = 5.92 Å, b = 7.59 Å, $\gamma \approx 90°$),[17,27] was then constructed and thermalized at 4000 K for 80 ps. The system was cooled following the annealing cycle 2-VIII proposed by Huff and co-workers.[39] The system was then thermalized at 300 K for 150 ps. The volume of the unit cell was kept constant in order to ensure the correct density of the

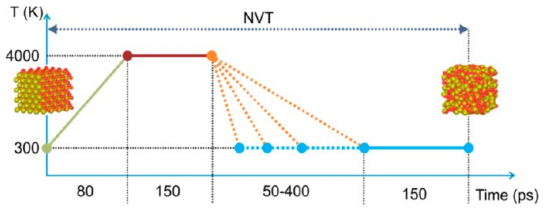

Figure 8. Illustration of the molecular dynamics protocol used to generate the amorphous bulk structures.

amorphous system, a key property in the description of the organic/inorganic electrostatic interactions. Four bulk αSiO_2 geometries were then created by setting the cooling times to 50, 100, 200, and 400 ps. The protocol is illustrated in Figure 8.

Amorphous silica slabs were then built from 2×2 supercells of the bulk samples. Periodicity was maintained along the *a* and *b* vectors, while a 20 Å vacuum layer was maintained on top of the amorphous structure. The slabs were relaxed at 1000 K for 50 ps in order to promote a reorganization of the surface atoms and then cooled to 300 K and thermalized for 100 ps. The four substrates, representing different realizations of an αSiO_2 surface, will be enumerated through the rest of this work as **1** (50 ps), **2** (100 ps), **3** (200 ps), and **4** (400 ps). We emphasize that the oxygen atoms exposed at the surface were not saturated with hydrogen atoms, and no water molecules were added on top of the slabs; this may have implications in comparison with the GIXD experiments, where all films were measured in ambient conditions.

$\alpha Si0_2$—Pentacene Interface. To examine the αSiO_2—pentacene interface, we constructed an $8 \times 8 \times 1$ pentacene supercell (128 molecules) and placed this layer 5.0 Å above the respective αSiO_2 surfaces. Simulations with 32, 128, and 556 pentacene molecules in the monolayer were performed to check for size dependence of the results on the supercell dimensions; it was found that the 128-molecule system provided a good compromise between the quality of the results and the computational time. Two starting conformations for the pentacene molecules in the monolayer were used: (i) a packing configuration to reproduce that obtained from X-ray diffraction experiments in ref 45 and (ii) all molecules set perfectly perpendicular to the surface as in ref 17. As we show later, the initial molecular packing configuration has no effect on the final layer morphology.

The αSiO_2—pentacene interfaces were built based on a unit cell matching the dimensions measured experimentally and energy minimized. This was followed by canonical NVT ensemble dynamics simulations that were run for 4 ns with a time step of 1 fs at a constant temperature of 300 K. During this procedure, all atoms in the silica slab were kept fixed in order to limit the computational cost; test simulations where the atoms in the αSiO_2 slab were allowed to move show no difference with regard to the final results. The charges of the Si and O atoms were kept constant at the final values optimized by the COMB potential. The pentacene atomic charges were fit to the electrostatic potential[46,47] calculated *via* density functional theory using the B3LYP[48] functional and the 6-311G** basis set in the Gaussian 09 software suite.[49] All pentacene molecules were treated at the atomistic level using the AMBER94[50] force-field, which has been successfully used to reproduce crystallographic structures, minimized geometries, and intermolecular energies predicted by different *ab initio* methodologies for a variety of nucleic acids and aromatic compounds.[51,52] The long-range interactions were described using a combination of the Buckingham and Coulomb potentials.[22] The intermolecular non-Coulomb terms were calculated using the number IV Williams parameters for C and H,[53] which reproduces well the crystalline structures and intermolecular vibrations of pentacene polymorphs as a function of temperature[54] and the crystal structures of naphthalene, anthracene, tetracene, and pentacene at different temperatures and pressures.[55−58] The non-Coulomb interactions between the silica and pentacene were described using the Dreiding force field[59] for the Si and O atoms. We applied the standard mixing rules—$A_{ij} = (A_{ii}A_{jj})^{1/2}$, $B_{ij} = (B_{ii} + B_{jj})/2$, $C_{ij} = (C_{ii}C_{jj})^{1/2}$—to determine the coefficients of the Buckingham equation. Periodic boundary conditions along *a* and *b* were applied, allowing the use of Ewald summation to compute the Coulomb interactions along these directions. The MD trajectory analysis and the molecular representations were performed using the MView suite.[60]

Conflict of Interest: The authors declare no competing financial interest.

Acknowledgment. The work at Georgia Tech was supported by the National Science Foundation under the Materials Research Science and Engineering (MRSEC) Program, Award Number DMR-0819885, with computing resources provided through the Chemistry Research Instrumentation and Facilities (CRIF) Program, Award Number CHE-0946869. D.W.B. gratefully acknowledges the Norwegian Research Council for financial support. Portions of this research were carried out at the Stanford Synchrotron Radiation Lightsource (SSRL), a Directorate of SLAC National Accelerator Laboratory and an Office of Science User Facility operated for the U.S. Department of Energy Office of Science by Stanford University. We thank Dr. Naga Rajesh Tummala for assisting with the ZINDO calculations and Professor C. Daniel Frisbie and Dr. Stefan Mannsfeld for valuable comments and discussion.

REFERENCES AND NOTES

1. Brédas, J.-L.; Beljonne, D.; Coropceanu, V.; Cornil, J. Charge-Transfer and Energy-Transfer Processes in Pi-Conjugated Oligomers and Polymers: a Molecular Picture. *Chem. Rev.* **2004**, *104*, 4971–5004.
2. Coropceanu, V.; Cornil, J.; da Silva Filho, D. A.; Olivier, Y.; Silbey, R.; Brédas, J.-L. Charge Transport in Organic Semiconductors. *Chem. Rev.* **2007**, *107*, 926–952.
3. Dodabalapur, A.; Torsi, L.; Katz, H. E. Organic Transistors: Two-Dimensional Transport and Improved Electrical Characteristics. *Science* **1995**, *268*, 270–271.
4. Park, B.-N.; Seo, S.; Evans, P. G. Channel Formation in Single-Monolayer Pentacene Thin Film Transistors. *J. Phys. D. Appl. Phys.* **2007**, *40*, 3506–3511.
5. Wang, S.; Kiersnowski, A.; Pisula, W.; Müllen, K. Microstructure Evolution and Device Performance in Solution-Processed Polymeric Field-Effect Transistors: The Key Role of the First Monolayer. *J. Am. Chem. Soc.* **2012**, *134*, 4015–4018.
6. Mas-Torrent, M.; Rovira, C. Novel Small Molecules for Organic Field-Effect Transistors: Towards Processability and High Performance. *Chem. Soc. Rev.* **2008**, *37*, 827–838.
7. Anthony, J. E.; Facchetti, A.; Heeney, M.; Marder, S. R.; Zhan, X. n-Type Organic Semiconductors in Organic Electronics. *Adv. Mater.* **2010**, *22*, 3876–3892.
8. Zaumseil, J.; Sirringhaus, H. Electron and Ambipolar Transport in Organic Field-Effect Transistors. *Chem. Rev.* **2007**, *107*, 1296–1323.
9. Braga, D.; Horowitz, G. High-Performance Organic Field-Effect Transistors. *Adv. Mater.* **2009**, *21*, 1473–1486.
10. Sirringhaus, H.; Bird, M.; Zhao, N. Charge Transport Physics of Conjugated Polymer Field-Effect Transistors. *Adv. Mater.* **2010**, *22*, 3893–3898.
11. Chen, H.-Y.; Hou, J.; Hayden, A. E.; Yang, H.; Houk, K. N.; Yang, Y. Silicon Atom Substitution Enhances Interchain Packing in a Thiophene-Based Polymer System. *Adv. Mater.* **2010**, *22*, 371–375.
12. Guo, Y.; Yu, G.; Liu, Y. Functional Organic Field-Effect Transistors. *Adv. Mater.* **2010**, *22*, 4427–4447.
13. Yun, Y.; Pearson, C.; Petty, M. C. Pentacene Thin Film Transistors with a Poly(methyl methacrylate) Gate Dielectric: Optimization of Device Performance. *J. Appl. Phys.* **2009**, *105*, 034508.
14. Kanbur, Y.; Irimia-Vladu, M.; Głowacki, E. D.; Voss, G.; Baumgartner, M.; Schwabegger, G.; Leonat, L.; Ullah, M.; Sarica, H.; Erten-Ela, S.; *et al.* Vacuum-Processed Polyethylene as a Dielectric for Low Operating Voltage Organic Field Effect Transistors. *Org. Electron.* **2012**, *13*, 919–924.
15. Nishikata, S.; Sazaki, G.; Sadowski, J.; Al-Mahboob, A.; Nishihara, T.; Fujikawa, Y.; Suto, S.; Sakurai, T.; Nakajima, K.

Polycrystalline Domain Structure of Pentacene Thin Films Epitaxially Grown on a Hydrogen-Terminated Si(111) Surface. *Phys. Rev. B* **2007**, *76*, 1–10.
16. Lanzilotto, V.; Sanchez-Sanchez, C.; Bavdek, G.; Cvetko, D.; Lopez, M. F.; Martin-Gago, J. A.; Floreano, L. Planar Growth of Pentacene on the Dielectric TiO_2 (110) Surface. *J. Phys. Chem. C* **2011**, *115*, 4664–4672.
17. Mannsfeld, S. C. B.; Virkar, A.; Reese, C.; Toney, M. F.; Bao, Z. Precise Structure of Pentacene Monolayers on Amorphous Silicon Oxide and Relation to Charge Transport. *Adv. Mater.* **2009**, *21*, 2294–2298.
18. Liu, S.; Wang, W. M.; Briseno, A. L.; Mannsfeld, S. C. B.; Bao, Z. Controlled Deposition of Crystalline Organic Semiconductors for Field-Effect-Transistor Applications. *Adv. Mater.* **2009**, *21*, 1217–1232.
19. Fritz, S. E.; Kelley, T. W.; Frisbie, C. D. Effect of Dielectric Roughness on Performance of Pentacene TFTs and Restoration of Performance with a Polymeric Smoothing Layer. *J. Phys. Chem. B* **2005**, *109*, 10574–10577.
20. Kalihari, V.; Tadmor, E. B.; Haugstad, G.; Frisbie, C. D. Grain Orientation Mapping of Polycrystalline Organic Semiconductor Films by Transverse Shear Microscopy. *Adv. Mater.* **2008**, *20*, 4033–4039.
21. Martinelli, N. G.; Savini, M.; Muccioli, L.; Olivier, Y.; Castet, F.; Zannoni, C.; Beljonne, D.; Cornil, J. Modeling Polymer Dielectric/Pentacene Interfaces: On the Role of Electrostatic Energy Disorder on Charge Carrier Mobility. *Adv. Funct. Mater.* **2009**, *19*, 3254–3261.
22. Della Valle, R. G.; Venuti, E.; Brillante, A.; Girlando, A. Molecular Dynamics Simulations for a Pentacene Monolayer on Amorphous Silica. *ChemPhysChem* **2009**, *10*, 1783–1788.
23. Yoneya, M.; Kawasaki, M.; Ando, M. Are Pentacene Monolayer and Thin-Film Polymorphs Really Substrate-Induced? A Molecular Dynamics Simulation Study. *J. Phys. Chem. C* **2012**, *116*, 791–795.
24. Käfer, D.; Ruppel, L.; Witte, G. Growth of Pentacene on Clean and Modified Gold Surfaces. *Phys. Rev. B* **2007**, *75*, 1–14.
25. Koch, N.; Gerlach, A.; Duhm, S.; Glowatzki, H.; Heimel, G.; Vollmer, A.; Sakamoto, Y.; Suzuki, T.; Zegenhagen, J.; Rabe, J. P.; *et al*. Adsorption-Induced Intramolecular Dipole: Correlating Molecular Conformation and Interface Electronic Structure. *J. Am. Chem. Soc.* **2008**, *130*, 7300–7304.
26. Lee, W. H.; Park, J.; Sim, S. H.; Lim, S.; Kim, K. S.; Hong, B. H.; Cho, K. Surface-Directed Molecular Assembly of Pentacene on Monolayer Graphene for High-Performance Organic Transistors. *J. Am. Chem. Soc.* **2011**, *133*, 4447–4454.
27. Schiefer, S.; Huth, M.; Dobrinevski, A.; Nickel, B. Determination of the Crystal Structure of Substrate-Induced Pentacene Polymorphs in Fiber Structured Thin Films. *J. Am. Chem. Soc.* **2007**, *129*, 10316–10317.
28. Minakata, T.; Imai, H.; Ozaki, M.; Saco, K. Structural Studies on Highly Ordered and Highly Conductive Thin Films of Pentacene. *J. Appl. Phys.* **1992**, *72*, 5220.
29. Dimitrakopoulos, C. D.; Brown, A. R.; Pomp, A. Molecular Beam Deposited Thin Films of Pentacene for Organic Field Effect Transistor Applications. *J. Appl. Phys.* **1996**, *80*, 2501.
30. Bouchoms, I.; Schoonveld, W. A.; Vrijmoeth, J.; Klapwijk, T. M. Morphology Identification of the Thin Film Phases of Vacuum Evaporated Pentacene on SiO_2 Substrates. *Synth. Met.* **1999**, *104*, 175–178.
31. Ruiz, R.; Nickel, B.; Koch, N.; Feldman, L.; Haglund, R.; Kahn, A.; Scoles, G. Pentacene Ultrathin Film Formation on Reduced and Oxidized Si Surfaces. *Phys. Rev. B* **2003**, *67*, 1–7.
32. Fritz, S. E.; Martin, S. M.; Frisbie, C. D.; Ward, M. D.; Toney, M. F. Structural Characterization of a Pentacene Monolayer on an Amorphous SiO_2 Substrate with Grazing Incidence X-ray Diffraction. *J. Am. Chem. Soc.* **2004**, *126*, 4084–4085.
33. Ruiz, R.; Mayer, A. C.; Malliaras, G. G.; Nickel, B.; Scoles, G.; Kazimirov, A.; Kim, H.; Headrick, R. L.; Islam, Z. Structure of Pentacene Thin Films. *Appl. Phys. Lett.* **2004**, *85*, 4926.
34. Yu, J.; Sinnott, S.; Phillpot, S. Charge Optimized Many-Body Potential for the Si/SiO_2 System. *Phys. Rev. B* **2007**, *75*, 1–13.
35. Shan, T.-R.; Devine, B. D.; Kemper, T. W.; Sinnott, S. B.; Phillpot, S. R. Charge-Optimized Many-Body Potential for the Hafnium/hafnium Oxide System. *Phys. Rev. B* **2010**, *81*, 1–12.
36. Plimpton, S. Fast Parallel Algorithms for Short-Range Molecular Dynamics. *J. Comput. Phys.* **1995**, *117*, 1–19.
37. Shan, T.-R.; Devine, B.; Hawkins, J.; Asthagiri, A.; Phillpot, S.; Sinnott, S. Second-Generation Charge-Optimized Many-Body Potential for Si/SiO_2 and Amorphous Silica. *Phys. Rev. B* **2010**, *82*, 1–9.
38. Shan, T.-R.; Devine, B.; Phillpot, S.; Sinnott, S. Molecular Dynamics Study of the Adhesion of Cu/SiO_2 Interfaces Using a Variable-Charge Interatomic Potential. *Phys. Rev. B* **2011**, *83*, 1–8.
39. Huff, N. Factors Affecting Molecular Dynamics Simulated Vitreous Silica Structures. *J. Non. Cryst. Solids* **1999**, *253*, 133–142.
40. Cruz-Chu, E. R.; Aksimentiev, A.; Schulten, K. Water-Silica Force Field for Simulating Nanodevices. *J. Phys. Chem. B* **2006**, *110*, 21497–21508.
41. Sarnthein, J.; Pasquarello, A.; Car, R. Structural and Electronic Properties of Liquid and Amorphous SiO_2: An Ab Initio Molecular Dynamics Study. *Phys. Rev. Lett.* **1995**, *74*, 4682–4685.
42. Soules, T. F.; Gilmer, G. H.; Matthews, M. J.; Stolken, J. S.; Feit, M. D. Silica Molecular Dynamic Force Fields—A Practical Assessment. *J. Non. Cryst. Solids* **2011**, *357*, 1564–1573.
43. Lopes, P. E. M.; Murashov, V.; Tazi, M.; Demchuk, E.; Mackerell, A. D. Development of an Empirical Force Field for Silica. Application to the Quartz-Water Interface. *J. Phys. Chem. B* **2006**, *110*, 2782–2792.
44. Schmahl, W. W.; Swainson, I. P.; Dove, M. T.; Graeme-Barber, A. Landau Free Energy and Order Parameter Behaviour of the Alpha; Beta; Phase Transition in Cristobalite. *Z. Kristallogr.* **1992**, *201*, 125.
45. Holmes, D.; Kumaraswamy, S.; Matzger, A. J.; Vollhardt, K. P. C. On the Nature of Nonplanarity in the [N]Phenylenes. *Chem.—Eur. J.* **1999**, *5*, 3399–3412.
46. Singh, U. C.; Kollman, P. A. An Approach to Computing Electrostatic Charges for Molecules. *J. Comput. Chem.* **1984**, *5*, 129–145.
47. Besler, B. H.; Merz, K. M.; Kollman, P. A. Atomic Charges Derived from Semiempirical Methods. *J. Comput. Chem.* **1990**, *11*, 431–439.
48. Stephens, P. J.; Devlin, F. J.; Chabalowski, C. F.; Frisch, M. J. Ab Initio Calculation of Vibrational Absorption and Circular Dichroism Spectra Using Density Functional Force Fields. *J. Phys. Chem.* **1994**, *98*, 11623–11627.
49. Frisch, M. J.; Trucks, G. W.; Schlegel, H. B.; Scuseria, G. E.; Robb, M. A.; Cheeseman, J. R.; Scalmani, G.; Barone, V.; Mennucci, B.; Petersson, G. A.; *et al*. *Gaussian 09*; Gaussian Inc., 2009.
50. Cornell, W. D.; Cieplak, P.; Bayly, C. I.; Gould, I. R.; Merz, K. M.; Ferguson, D. M.; Spellmeyer, D. C.; Fox, T.; Caldwell, J. W.; Kollman, P. A. A Second Generation Force Field for the Simulation of Proteins, Nucleic Acids, and Organic Molecules. *J. Am. Chem. Soc.* **1995**, *117*, 5179–5197.
51. Wang, J.; Cieplak, P.; Kollman, P. A. How Well Does a Restrained Electrostatic Potential (RESP) Model Perform in Calculating Conformational Energies of Organic and Biological Molecules? *J. Comput. Chem.* **2000**, *21*, 1049–1074.
52. Wang, J.; Wolf, R. M.; Caldwell, J. W.; Kollman, P. A.; Case, D. Development and Testing of a General Amber Force Field. *J. Comput. Chem.* **2004**, *25*, 1157–1174.
53. Williams, D. E. Nonbonded Potential Parameters Derived from Crystalline Hydrocarbons. *J. Chem. Phys.* **1967**, *47*, 4680.
54. Della Valle, R. G.; Venuti, E.; Farina, L.; Brillante, A.; Masino, M.; Girlando, A. Intramolecular and Low-Frequency Intermolecular Vibrations of Pentacene Polymorphs as a Function of Temperature. *J. Phys. Chem. B* **2004**, *108*, 1822–1826.
55. Venuti, E.; Della Valle, R. G.; Brillante, A.; Masino, M.; Girlando, A. Probing Pentacene Polymorphs by Lattice Dynamics Calculations. *J. Am. Chem. Soc.* **2002**, *124*, 2128–2129.

56. Venuti, E.; Della Valle, R.; Farina, L.; Brillante, A.; Masino, M.; Girlando, A. Phonons and Structures of Tetracene Polymorphs at Low Temperature and High Pressure. *Phys. Rev. B* **2004**, *70*, 1–8.
57. Guido, R.; Valle, D.; Venuti, E.; Brillante, A. Pressure and Temperature Effects in Lattice Dynamics: the Case of Naphthalene. *Chem. Phys.* **1995**, *198*, 79–89.
58. Oehzelt, M.; Aichholzer, a.; Resel, R.; Heimel, G.; Venuti, E.; Della Valle, R. Crystal Structure of Oligoacenes Under High Pressure. *Phys. Rev. B* **2006**, *74*, 1–7.
59. Mayo, S. L.; Olafson, B. D.; Goddard, W. A. DREIDING: a Generic Force Field for Molecular Simulations. *J. Phys. Chem.* **1990**, *94*, 8897–8909.
60. Viani, L. MView: A Tool for Visualization and Analysis of Molecular Properties, Www.mview-Tools.com.
61. Mozzi, R. L.; Warren, B. E. The Structure of Vitreous Silica. *J. Appl. Crystallogr.* **1969**, *2*, 164–172.
62. Connolly, M. L. Analytical Molecular Surface Calculation. *J. Appl. Crystallogr.* **1983**, *16*, 548–558.
63. Breiby, D. W.; Bunk, O.; Pisula, W.; Sølling, T. I.; Tracz, A.; Pakula, T.; Müllen, K.; Nielsen, M. M. Structure of Zone-Cast HBC-$C_{12}H_{25}$ Films. *J. Am. Chem. Soc.* **2005**, *127*, 11288–11293.
64. Breiby, D. W.; Bunk, O.; Andreasen, J. W.; Lemke, H. T.; Nielsen, M. M. Simulating X-Ray Diffraction of Textured Films. *J. Appl. Crystallogr.* **2008**, *41*, 262–271.
65. Vineyard, G. Grazing-Incidence Diffraction and the Distorted-Wave Approximation for the Study of Surfaces. *Phys. Rev. B* **1982**, *26*, 4146–4159.
66. Robinson, I. Crystal Truncation Rods and Surface Roughness. *Phys. Rev. B* **1986**, *33*, 3830–3836.
67. Lin, Y.-Y.; Gundlach, D. J.; Nelson, S. F.; Jackson, T. N. Stacked Pentacene Layer Organic Thin-Film Transistors with Improved Characteristics. *IEEE Electron Device Lett.* **1997**, *18*, 606–608.
68. Brédas, J.-L.; Calbert, J. P.; da Silva Filho, D. A.; Cornil, J. Organic Semiconductors: A Theoretical Characterization of the Basic Parameters Governing Charge Transport. *Proc. Natl. Acad. Sci. U.S.A.* **2002**, *99*, 5804–5809.
69. Delgado, M. C. R.; Kim, E.; da Silva Filho, D. A.; Bredas, J. Tuning the Charge-Transport Parameters of Perylene Diimide Single Crystals *via* End And/or Core Functionalization: a Density Functional Theory Investigation. *J. Am. Chem. Soc.* **2010**, *132*, 3375–3387.
70. Cornil, J.; Calbert, J. P.; Brédas, J. L. Electronic Structure of the Pentacene Single Crystal: Relation to Transport Properties. *J. Am. Chem. Soc.* **2001**, *123*, 1250–1251.
71. Ridley, J.; Zerner, M. C. An Intermediate Neglect of Differential Overlap Technique for Spectroscopy: Pyrrole and the Azines. *Theor. Chim. Acta* **1973**, *32*, 111–134.
72. Zerner, M. C.; Loew, G. H.; Kirchner, R. F.; Mueller-Westerhoff, U. T. An Intermediate Neglect of Differential Overlap Technique for Spectroscopy of Transition-Metal Complexes. Ferrocene. *J. Am. Chem. Soc.* **1980**, *102*, 589–599.
73. Giri, G.; Verploegen, E.; Mannsfeld, S. C. B.; Atahan-Evrenk, S.; Kim, D. H.; Lee, S. Y.; Becerril, H. A.; Aspuru-Guzik, A.; Toney, M. F.; Bao, Z. Tuning Charge Transport in Solution-Sheared Organic Semiconductors Using Lattice Strain. *Nature* **2011**, *480*, 504–508.
74. Tseng, H.-R.; Ying, L.; Hsu, B. B. Y.; Perez, L. A.; Takacs, C. J.; Bazan, G. C.; Heeger, A. J. High Mobility Field Effect Transistors Based on Macroscopically Oriented Regioregular Copolymers. *Nano Lett.* **2012**, *12*, 6353–6357.
75. van de Craats, A. M.; Stutzmann, N.; Bunk, O.; Nielsen, M. M.; Watson, M.; Müllen, K.; Chanzy, H. D.; Sirringhaus, H.; Friend, R. H. Meso-Epitaxial Solution-Growth of Self-Organizing Discotic Liquid-Crystalline Semiconductors. *Adv. Mater.* **2003**, *15*, 495–499.